PHOTON PROPAGATION AROUND COMPACT OBJECTS AND THE INFERRED PROPERTIES OF THERMALLY EMITTING NEUTRON STARS

Dimitrios Psaltis, Feryal Özel, and Simon DeDeo
Harvard-Smithsonian Center for Astrophysics, 60 Garden St., Cambridge, MA 02138;
dpsaltis, fozel, sdedeo@cfa.harvard.edu

Draft version May 3, 2000

ABSTRACT

Anomalous X-ray pulsars, compact non-pulsing X-ray sources in supernova remnants, and X-ray bursters are three distinct types of sources for which there are viable models that attribute their X-ray emission to thermal emission from the surface of a neutron star. Inferring the surface area of the emitting regions in such systems is crucial in assessing the viability of different models and in providing bounds on the radii of neutron stars. We show that the spectroscopically inferred areas of the emitting regions may be over- or under-estimated by a factor of $\lesssim 2$, because of the three-dimensional geometry of the system and general relativistic light deflection, combined with the effects of phase averaging. Such effects make the determination of neutron-star radii uncertain, especially when compared to the $\sim 5\%$ level required for constraining the equation of state of neutron-star matter. We also note that, for a given spectral shape, the inferred source luminosities and pulse fractions are anticorrelated because they depend on the same properties of the emitting regions, namely their sizes and orientations. As a result, brighter sources have on average weaker pulsation amplitudes than fainter sources. We argue that this property can be used as a diagnostic tool in distinguishing between different spectral models. As an example, we show that the high inferred pulse fraction and brightness of the pulsar RXS J1708−40 are inconsistent with isotropic thermal emission from a neutron-star surface. Finally, we discuss the implication of our results for surveys in the soft X-rays for young, cooling neutron stars in supernova remnants and show that the absence of detectable pulsations from the compact source at the center of Cas A (at a level of $\gtrsim 30\%$) is not a strong argument against its identification with a spinning neutron star.

Subject headings: relativity — stars: neutron — X-rays: stars

1. INTRODUCTION

Neutron stars in nature appear in various different flavors. They were first unambiguously discovered in radio wavelengths as rotation-powered pulsars and later on, in X-rays, as accretion-powered pulsars and bursters. Such systems, however, constitute only a small fraction of the expected number of neutron stars in the galaxy, as inferred from estimates of supernova rates (e.g., Kaspi 2000). As a result, ongoing searches exist for detecting neutron stars in different manifestations, e.g., as isolated stars accreting from the interstellar medium (e.g., Belloni et al. 1997) or simply cooling by thermal emission (e.g., Pavlov et al. 1996). Different emission mechanisms are thought to operate in different types of neutron stars and possibly even between different wavelength bands in a given system. For at least three distinct classes of neutron stars, which we discuss below, viable models exist in which radiation emerging directly from their surfaces is responsible for their high-energy spectra.

A number of slow X-ray pulsars, often called the anomalous X-ray pulsars (AXPs; Mereghetti & Stella 1995) form a distinct class of neutron stars with soft X-ray spectra but no radio or optical counterparts. Because of their high spin-down rates and association with supernova remnants (SNRs) they are thought to be young and related to the soft γ-ray repeaters, in their quiescent states (see Hurley 2000). It is still an open question whether such objects are neutron stars accreting from a fossil disk (e.g., van Paradijs et al. 1996; Chaterjee, Narayan, & Hernquist 2000), are powered by magnetospheric emission (e.g., Thompson & Duncan 1995, 1996), or even emitting thermally (Heyl & Hernquist 1998).

Another class of objects, potentially related to the AXPs are the compact, non-pulsing, soft X-ray sources that are being discovered within SNRs. The most recent of such compact objects is the central source in Cas A discovered with the *Chandra X-ray Observatory* (Tananbaum 1999; see also Pavlov et al. 2000; Chakrabarty et al. 2000). Their spectra and luminosities are typical of what is expected for cooling, young neutron stars (see also Pavlov et al. 1996; Zavlin et al. 1998, 1999). However, the absence of coherent pulsations in their X-ray brightness allows for the possibility that they are black holes accreting from fall-back material (see, e.g., Pavlov et al. 2000; Chakrabarty et al. 2000).

Finally, weakly-magnetic ($\lesssim 10^{10}$ G) accreting neutron stars often show thermal emission from their surfaces during thermonuclear flashes, the so-called Type I X-ray bursts (see Lewin, van Paradijs, & Taam 1996). In six bursters, relatively coherent oscillations are detected during the bursts, at frequencies $\sim$ 300 Hz (see, e.g., Strohmayer et al. 1996). The coherence and stability of the oscillations suggests that they occur at the neutron-star spin frequencies and are caused by the non-uniform pattern of burning in their surface layers.

Understanding the properties of the X-ray emission from such thermally emitting neutron stars, especially in connection to the presence or absence of detectable coherent pulsations, is crucial in assessing the viability of different

models. Moreover, comparing model spectra to observations offers the possibility of measuring the radii of neutron stars and hence constraining the properties of neutron-star matter (see Lattimer & Prakash 2000 for a recent discussion). Recently, there has been significant progress in calculating spectra emerging from neutron-star atmospheres with various compositions (see, e.g., Pavlov et al. 1996; Heyl & Hernquist 1998). Constraints on the amplitudes of oscillations from compact stars with non-uniform surface emission have also been studied in connection to the observed oscillation amplitudes in cooling radio pulsars (Page 1995), bursters (see, e.g., Miller, & Lamb 1998; Weinberg, Miller, & Lamb 2000), and AXPs (DeDeo, Psaltis, & Narayan 2000).

In this article, we address a number of issues related to the emission from a spinning neutron-star with a non-uniform surface brightness. In particular, in §2 we study the effects of the three-dimensional geometry of the systems, phase averaging, and the general relativistic deflection of light. In §3, we demonstrate that, when the radiation emerges from a localized surface area on a rotating star, the radiation flux reaching an observer at infinity may be substantially different compared to the case of isotropic, spherically symmetric emission from a compact star with the same surface area (see also Zavlin, Shibanov, & Pavlov 1995). As a result, when such effects are not taken explicitly into account, the hot-spot sizes, inferred from the observed fluxes and temperatures, may be significantly over- or under-estimated. We show that general-relativistic deflection typically reduces this discrepancy, depending on the compactness of the neutron star.

We also note that the surface area on the neutron star, from which the localized emission emerges, determines both the flux that reaches the observer at infinity and the amplitude of pulsations at the stellar spin frequency. In fact, for stars with the same local surface temperature and emerging spectrum, an anticorrelation is expected between the luminosity and pulsation amplitude. Therefore, simultaneous consideration of these two properties for a given system can offer strong constraints on the operating emission mechanisms. In §4, we investigate this property and its implications for the observations of compact X-ray sources with and without detectable pulsations.

2. THE BRIGHTNESS OF A SPINNING NEUTRON STAR

In this section, we calculate the phase-averaged radiation flux that reaches an observer at infinity from the surface of a spinning neutron star (or other compact object) with a non-uniform surface brightness, following the procedure outlined by Pechenick, Ftaclas, & Cohen (1983; see DeDeo et al. 2000 for the details of our implementation). Throughout this article, we neglect any interaction of photons with matter between the surface of the neutron star and the observer, as well as any polarization effects (see, e.g., Shaviv, Heyl, & Lithwick 1999). We also assume that the star is slowly rotating, so that its spacetime is described by the Schwarzschild metric. Finally, we set $c = G = 1$, where c is the speed of light and G is the gravitational constant.

We specify, as a boundary condition, the specific intensity $I(\theta, \phi, \theta')$ of radiation emerging from the neutron-star surface, evaluated at the local rest frame and integrated over all photon energies. The polar coordinates (θ, ϕ) determine the position on the stellar surface with respect to the rotation axis, while the angle θ' is measured locally with respect to the radial direction. Hereafter, we assume that the emission is isotropic and hence that the specific intensity is independent of θ'. This choice leads to the strongest effects of general relativistic light deflection, even though it is not necessarily the most appropriate for thermal emission from a neutron star (see, e.g., Zavlin et al. 1998). Calculating in detail the beaming of radiation requires the knowledge of the temperature stratification of the neutron-star atmosphere and the solution of the resulting radiative-transfer problem, which is beyond the scope of this paper but will reported elsewhere.

The brightness distribution on the neutron star surface depends on the emission process under consideration (i.e., thermal cooling versus localized nuclear burning), the surface profile of its magnetic field (see, e.g., Heyl & Hernquist 1998), and the possible presence of lateral metallicity gradients (see, e.g., Pavlov et al. 2000). For the purposes of our analysis, considering a geometry of two antipodal hot spots of variable size with uniform surface brightness captures the relevant properties of these different processes. Following the notation used for radio pulsars (e.g., Lyne & Graham-Smith 1990), we denote the half-opening angle of each spot by ρ, its angular distance from the rotation pole by α, and the emerging constant specific intensity by $I_{\rm NS}$.

The flux measured by an observer at distance d, whose polar coordinates with respect to the stellar rotation axis are denoted by (β, Φ), is given by (Pechenick et al. 1983, eq. [3.15])

$$F_\infty(\beta,\Phi) = I_{\rm NS}\left(\frac{R_{\rm NS}}{d}\right)^2\left(\frac{M_{\rm NS}}{R_{\rm NS}}\right)^2 \times \left(\sqrt{-g_{00}}\right)^4 \int_0^{x_{\rm max}} h[\theta(x,\beta);\rho,\theta_0]x dx \; . \quad (1)$$

Here, $M_{\rm NS}$ and $R_{\rm NS}$ are the neutron-star mass and radius, $g_{00} \equiv -(1 - 2M_{\rm NS}/R_{\rm NS})$ for a Schwarzschild spacetime, $x_{\rm max} \equiv (R_{\rm NS}/M_{\rm NS})/\sqrt{-g_{00}}$, and the function $h(\theta;\rho,\theta_0)$ is defined in Pechenick et al. (1983, eq. [3.3]). The angle θ_0 measures the distance on the stellar surface between the center of one of the hot spots and the direction to the observer, and is given by

$$\cos\theta_0 = \sin\alpha\sin\beta\cos\Phi + \cos\alpha\cos\beta \; . \quad (2)$$

Equation (1) is simply the integral of specific intensities, at the distance of the observer, over the impact parameters $b = xM_{\rm NS}$ of rays that are parallel at radial infinity. The angle $\theta(x,\beta)$ at which each parallel ray intersects the stellar surface is found by integrating the photon trajectory from radial infinity to the stellar surface, i.e.,

$$\theta = \int_0^{M_{\rm NS}/R_{\rm NS}} [x^{-2} - (1-2u)u^2]^{-1/2} du \quad (3)$$

(Pechenick et al. 1983).

The average flux, measured by an observer at infinity, averaged over a time longer than the rotational period of the neutron star, simply is

$$F_\infty = \pi I_{\rm NS}\left(\sqrt{-g_{00}}\right)^2 A(\alpha,\beta,\rho,p)\left(\frac{R_{\rm NS}}{d}\right)^2 \; , \quad (4)$$

where $p \equiv R_{\rm NS}/2M_{\rm NS}$ and we have defined

$$A(\alpha,\beta,\rho,p) \equiv \left(\frac{-g_{00}}{2\pi^2 p^2}\right)\int_0^{2\pi} d\Phi \int_0^{x_{\rm max}} h[\theta(x,\beta);\alpha,\theta_0]xdx \ . \tag{5}$$

When the local radiation spectrum emerging from the stellar surface is that of a blackbody of temperature $T_{\rm NS}$, then $\pi I_{\rm NS} = \sigma T_{\rm NS}^4$, where σ is the Stefan-Boltzmann constant.

If the emission were spherically symmetric, an observer at radial infinity would measure a specific intensity $I_\infty = (-g_{00})I_{\rm NS}$ and a blackbody temperature $T_\infty = (\sqrt{-g_{00}})T_{\rm NS}$. In the absence of any prior information about the opening angle of the hot spots and their orientation, an observer at infinity would therefore infer for the emitting region a surface area

$$S_\infty \equiv \frac{4d^2F_\infty}{I_\infty} = 4\pi d^2\frac{F_\infty}{\sigma T_\infty^4} \ . \tag{6}$$

It is then customary to assume a given neutron-star mass and radius and correct for the effect of gravitational redshifts as (see, e.g., Lattimer & Prakash 2000)

$$S_{\rm inf} \equiv (-g_{00})S_\infty = (-g_{00})4\pi d^2\frac{F_\infty}{\sigma T_\infty^4} \ . \tag{7}$$

Given that the real surface area of two polar caps of half-opening angle ρ is $S_{\rm pc} = 4\pi(1-\cos\rho)R_{\rm NS}^2$, we conclude that the error in the estimate of the emitting area is

$$\frac{S_{\rm inf}}{S_{\rm pc}} = \frac{1}{1-\cos\rho}A(\alpha,\beta,\rho,p) \ . \tag{8}$$

As a consequence, estimating the radius of the polar cap according to $\pi D_{\rm inf}^2 \equiv S_{\rm inf}$, leads to an error with respect to the real polar cap radius $D_{\rm pc} = \rho R_{\rm NS}$ equal to

$$\frac{D_{\rm inf}}{D_{\rm pc}} = \sqrt{\frac{2A(\alpha,\beta,\rho,p)}{\rho^2}} \ . \tag{9}$$

Finally, assuming that the whole neutron star is emitting uniformly and using equation (7) to infer its radius, results in an error equal to

$$\frac{R_{\rm inf}}{R_{\rm NS}} = A(\alpha,\beta,\rho,p) \ . \tag{10}$$

3. RESULTS

3.1. *Uncertainties in the Inferred Surface Areas of the Emission Regions*

We present in this section the uncertainties introduced to the estimates of the spectroscopically inferred polar-cap surface areas by the three-dimensional geometry of the problem, the effects of phase averaging, and the general relativistic light deflection.

Figures 1 and 2 show the ratio of the inferred to the intrinsic surface areas of the polar caps, for different opening angles, neutron-star radii, and orientations of the rotation axis with respect to the polar caps and the observer. For neutron-stars that are not very relativistic ($p = 4$), the inferred surface areas can be significantly over- or under-estimated, depending on the relative orientations of the polar caps and the observer. In order to understand this effect, we calculate explicitly the ratio $S_{\rm inf}/S_{\rm pc}$ for the limiting case of a Newtonian star, an infinitesimally small emitting area, and two specific orientations.

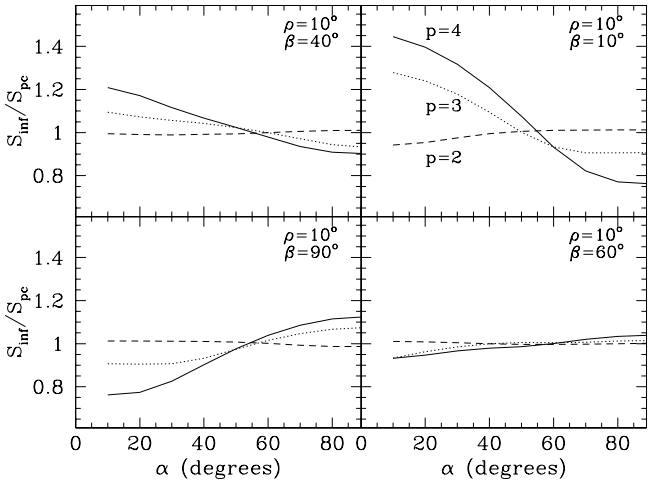

FIG. 1.— Ratio of spectroscopically inferred polar-cap surface area $S_{\rm inf}$ to their intrinsic area $S_{\rm pc}$, as a function of the orientation of the polar caps (α), for various values of the observer inclination (β) with respect to the rotational axis and for different neutron-star radii. The opening angle ρ of each polar cap is held fixed at 10 degrees.

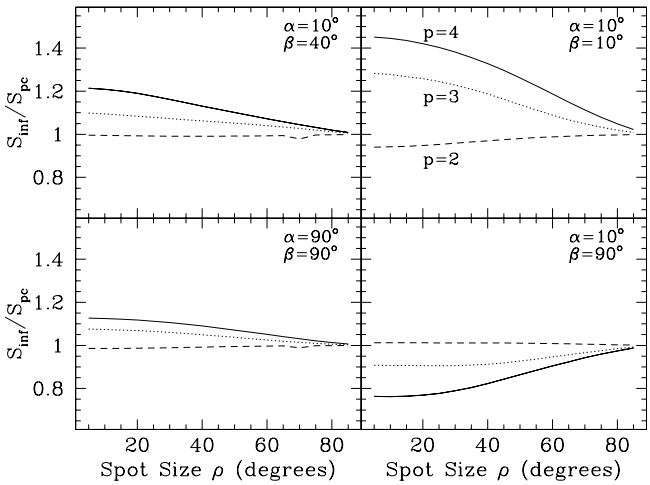

FIG. 2.— Same as in Figure 1 but as a function of the opening angle ρ of each polar cap.

When $\alpha = \beta = 0°$, one polar cap always appears at the geometric center of the stellar disk, and the flux measured at infinity is time independent. In this case, $\cos\theta_0 = 1$ and, by symmetry,

$$h[\theta(\chi,\beta);\rho\to 0,\theta_0 = 0°] = 2\pi \ . \tag{11}$$

Using these values in evaluating the integral (5), we obtain

$$A(\alpha=\beta=0°,\rho\to 0,p\to\infty) = 2(1-\cos\rho) \tag{12}$$

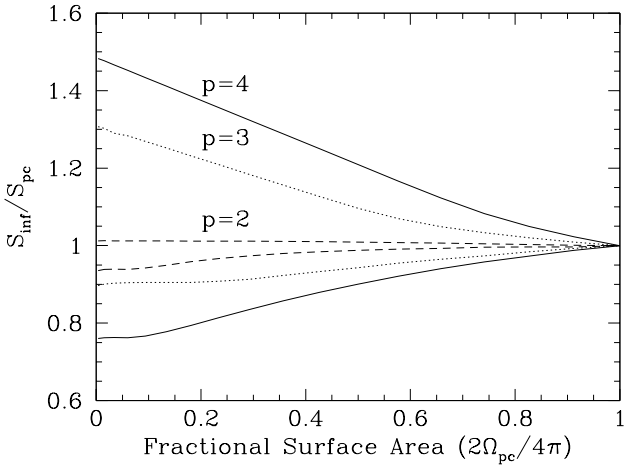

FIG. 3.— Bounds on the ratio of the inferred $S_{\rm inf}$ to the intrinsic size $S_{\rm pc}$ of emitting polar caps, for different emitting fractions of the stellar surface and neutron-star radii.

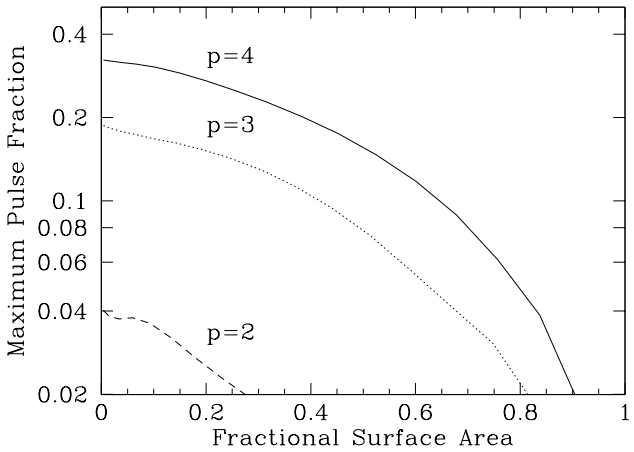

FIG. 4.— Maximum pulse fraction of the brightness of a spinning neutron star, for different emitting fractions of the stellar surface and neutron-star radii.

which gives $S_{\rm inf}/S_{\rm pc} = 2$. When, on the other hand, $\alpha = 0^\circ$ and $\beta = 90^\circ$, $\cos\theta_0 = 0$, the polar caps are being viewed only at grazing angles. In this case,

$$h[\theta(\chi,\beta);\rho\to 0,\theta_0 = 90^\circ]\chi \to 0, \tag{13}$$

and

$$A(\alpha = 0^\circ,\beta = 90^\circ,\rho\to 0,p\to\infty)\to 0 \tag{14}$$

and hence $S_{\rm inf}/S_{\rm pc}\to 0$. As a result, for a Newtonian star and an infinitesimally small emitting area,

$$0 \le \frac{S_{\rm inf}}{S_{\rm pc}} \le 2\,. \tag{15}$$

For increasingly more compact neutron stars, i.e., for decreasing values of p, the error in the estimate of the emitting area decreases substantially, reaching $\lesssim 5\%$ when $p = 2$. This is the result of the strong gravitational light bending near the neutron star surface, which efficiently redistributes the emitting photons to almost all directions of propagation, mimicking the spherically symmetric case.

Figure 3 shows the maximum and minimum of the ratio $S_{\rm inf}/S_{\rm pc}$ for all possible orientations of the hot spot and the observer, as a function of the fractional emitting surface area ($S_{\rm pc}/4\pi R_{\rm NS}^2 = 2\Omega_{\rm pc}/4\pi$) of the neutron-star surface, for different neutron-star radii. As expected, in all cases, the maximum corresponds to $\alpha = \beta = 0^\circ$ and the minimum to $\alpha = 0^\circ$ and $\beta = 90^\circ$, and they both converge to unity as $\Omega_{\rm pc}\to 2\pi$. However, for small polar caps and typical neutron-star masses and radii, there is a factor of $\lesssim 2$ spread in the systematic uncertainty in the estimated area of the emitting region.

3.2. *Trends Between the Pulse Fractions and Luminosities of Thermally Emitting Neutron Stars*

The X-ray brightness of a spinning neutron-star with a non-uniform surface emission shows pulsations at the stellar spin frequency and its harmonics. Just as in the case of the flux observed at infinity, the amplitude of pulsations as well as the harmonic structure also depend strongly on the brightness distribution on the stellar surface and the degree of gravitational light bending. Therefore, inevitable trends exist between the pulse fractions and the brightness of a source, as we discuss below.

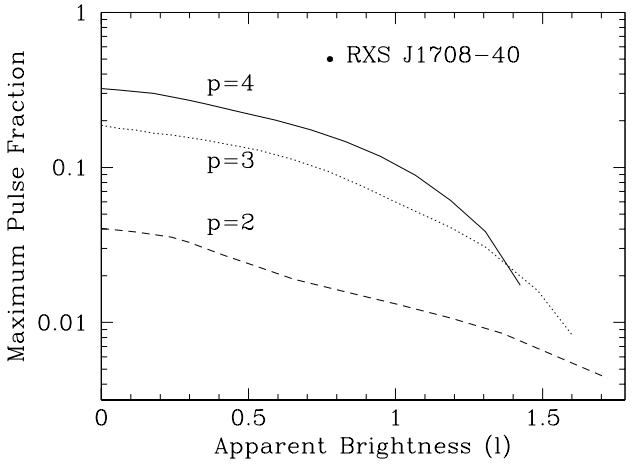

FIG. 5.— Maximum allowed pulse fraction from a spinning neutron star as a function of its apparent brightness [$l = (4\pi d^2 F_\infty/10^{36}\ {\rm erg\ s^{-1}})/(T_\infty/0.5\ {\rm keV})$] inferred by an observer at infinity, assuming that the emission is spherically symmetric and without applying any redshift corrections. The local radiation spectrum is assumed to be that of a blackbody and the radius of the neutron star is fixed at 10 km. Different relativity parameters correspond to different neutron-star masses. The data point correspond to the X-ray pulsar RXS J1708−40.

For the case of two antipodal polar caps discussed here, the amplitude of pulsations from a neutron star of a given radius decreases with increasing polar-cap surface area and increasing mass. This is shown in Figure 4, where the pulse fraction, defined as

$$PF \equiv \frac{F(\Phi)|_{\rm max} - F(\Phi)|_{\rm min}}{F(\Phi)|_{\rm max} + F(\Phi)|_{\rm min}}\,, \tag{16}$$

is plotted against the fractional surface area of the emitting region, for different neutron-star radii.

As it has already been discussed extensively in the literature, for the isotropic beaming we use here, general relativistic light bending suppresses the pulse fraction below

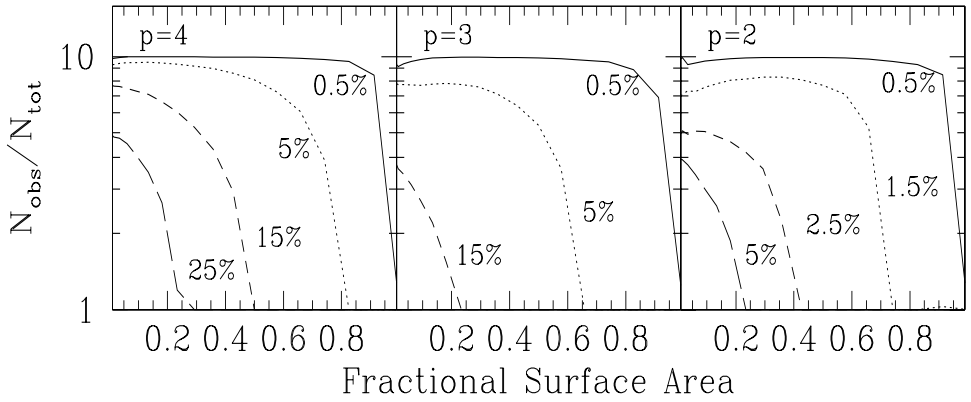

FIG. 6.— Fraction $N_{\rm obs}/N_{\rm tot}$ of observed systems with pulse fraction larger than a given threshold as a function of the fractional size of the polar caps, for different neutron-star radii.

$\sim 35\%$, even for infinitesimally small polar-cap sizes. As a result, detection of a pulsation from a neutron star with a larger amplitude severely constrains any such models of emission from the stellar surface. However, these constraints may become even tighter if the observed brightness of the neutron star is also taken into account. For the same local radiation spectrum, small polar-cap sizes correspond to large pulse fractions but weak radiation fluxes and vice versa. As a result, in this case, the maximum pulse fraction for a bright source is significantly smaller compared to the maximum pulse fraction for a faint source.

Inferring the fractional surface area of the emitting region, and thus the source brightness, requires an a priori knowledge of the orientation of the polar caps and the observer with respect to the rotation axis, which are almost always unknown. For example, a given observed source brightness may be the result of a small polar cap viewed from a favorable orientation ($\alpha \sim \beta \sim 0^\circ$) or of a larger polar cap viewed from an unfavorable orientation ($\alpha \sim \beta \sim 90^\circ$). Therefore, since the observed brightness does not have an one-to-one correspondence with the fractional emitting surface area, the constraints plotted in Figure 4 cannot be compared directly with observations. However, although both configurations in the above example may produce the same pulse-average flux as measured by the observer, the first configuration typically produces a significantly smaller pulse fraction. As a result, the combination of these two properties, namely the source brightness and pulse fraction, provide us with a useful diagnostic tool, as we discuss below.

We can simultaneously account for all the above effects if we assume a particular model of the local radiation spectrum and search for the maximum pulse fraction as a function of the brightness of the source measured by an observer at infinity. As an example, we assume that the local radiation spectrum at each point on the polar caps is that of a blackbody of temperature $T_{\rm NS}$ with isotropic beaming. An observer at infinity, would observe a radiation flux F_∞, and making the assumption that the emission is spherically symmetric, would infer a luminosity

$$L_\infty = 4\pi d^2 F_\infty \ . \tag{17}$$

According to equation [4], this luminosity is

$$L_\infty = 4\pi R_{\rm NS}^2 \sigma T_{\rm NS}^4 \left(\sqrt{-g_{00}}\right)^2 A(\alpha,\beta,\gamma,r) \ , \tag{18}$$

where $T_{\rm NS} = T_\infty/(\sqrt{-g_{00}})$. We define an apparent brightness as

$$l \equiv \left(\frac{4\pi d^2 F_\infty}{10^{36}\ {\rm erg\ s^{-1}}}\right)\left(\frac{T_\infty}{0.5\ {\rm keV}}\right)^{-4} , \tag{19}$$

which is a function of only observed quantities and is independent of the neutron-star temperature in our model calculations. We use this quantity as a measure of the brightness of the star at infinity and, in Figure 5, we plot against it the maximum pulse fraction for a 10 km neutron star emitting a blackbody spectrum. This figure shows clearly that, even though emission from a neutron-star surface can in principle produce pulse fractions as large as $\sim 30\%$ (for very small hot spots), it can never produce, e.g., a pulse fraction of $\gtrsim 10\%$ simultaneously with an inferred luminosity of $\gtrsim 10^{36}$ erg s^{-1} for a 0.5 keV blackbody temperature.

4. DISCUSSION

In this paper we have shown that the inferred properties of thermally emitting neutron stars, i.e., their emitting surface areas and pulse fractions, are significantly affected by the three-dimensional geometry of the systems, phase-averaging effects, and general relativistic light bending. The uncertainties introduced by these effects can be significant (with a spread of $\lesssim 2$), especially at the limit of small emitting surface areas. However, even when most of the neutron star surface is emitting, the uncertainties in estimating the neutron-star radius are of the same order as the $\sim 5\%$ level required (Lattimer & Prakash 2000) for constraining the equation of state of neutron-star matter.

We have also argued that for a given local radiation spectrum emerging from a bright spot on the stellar surface, faint sources can give rise to larger pulse fractions than brighter sources. The maximum pulse fraction as a function of the brightness of the neutron star, measured by l (cf. eq. [19]), provides a diagnostic tool for distinguishing between different emission models. These derived constraints depend both on the local radiation spectrum

(e.g., thermal versus non-thermal emission) and its beaming and are, therefore, different for different classes of models. Moreover, both quantities are measurable from spectral and timing observations and can be directly compared to the calculated constraints. The high observed pulse fractions of AXPs (see, e.g., Chakrabarty et al. 2000) and X-ray bursters (Strohmayer et al. 1998) have been shown to strongly constrain emission models and such constraints can become only tighter when the apparent luminosities of these systems are also taken into account. As an example, we consider the source RXS J1708−40, which has been identified as an AXP (Sugizaki et al. 1997). Fitting a blackbody spectrum to *ASCA* observations of this source gives a temperature of $T_\infty = 0.41 \pm 0.03$ keV and a blackbody flux of $4\pi d^2 F_\infty = 3.16 \times 10^{35}$ erg s^{-1} (Sugizaki et al. 1997; Chakrabarty et al. 2000). The inferred apparent brightness of this source is, therefore, $l = 0.8$ and combined with the observed $\simeq 50\%$ pulse fraction (Sugizaki et al. 1997) is inconsistent with isotropic thermal emission from the neutron-star surface (see Fig. 5).

Finally, our results also have a number of important implications for soft X-ray surveys, in supernova remnants, for young, cooling neutron stars that emit thermally. For a given spectral shape, the brightest sources, which would be more easily detectable, correspond to smaller pulse fractions, while strong pulsations are only expected from dimmer sources. This effect is shown in Figure 6, where the fraction of systems $N_{\rm obs}/N_{\rm tot}$ with a pulse fraction at infinity larger than a threshold PF_0 is plotted against the fractional emitting surface area. For this purpose, we assume a random orientation of the magnetic inclination and the inclination to the observer for a sample of systems and define

$$\frac{N_{\rm obs}}{N_{\rm tot}}(PF_0) = \int_{\alpha=0}^{\pi/2}\int_{\alpha=0}^{\pi/2}[PF(\alpha,\beta) > PF_0]\alpha d\alpha\ \beta d\beta\ . \quad (20)$$

For realistic neutron star masses and radii ($p \sim 2-3$), only a very small fraction of sources shows pulsations that are detectable at a significant level ($\gtrsim 10-20\%$) and this fraction drops rapidly with increasing apparent luminosity.

If the central source in the remnant Cas A is a young, cooling neutron star, its surface brightness distribution cannot be uniform, as inferred from fitting thermal models to the observed countrate spectra (Pavlov et al. 2000; Chakrabarty et al. 2000). However, as Figure 6 shows, this property is not inconsistent with the $\simeq 30\%$ upper limit on its pulse fraction (Chakrabarty et al. 2000). For the assumed isotropic beaming of the emerging radiation and the very small fractional surface area inferred for the central source in Cas A (Pavlov et al. 2000; Chakrabarty et al. 2000), less than half of the systems would have been detected with pulse fractions higher than the detection threshold, if $p = 4$. For more realistic neutron-star properties ($p = 2, 3$), no system would show such a large pulse fraction. Therefore, the absence of detectable pulsations from this source is not a strong argument against its identification with a spinning neutron star.

We thank Deepto Chakrabarty, Lars Hernquist, and Ramesh Narayan for many useful discussions. D. P. acknowledges support of a post-doctoral fellowship from the Smithsonian Insitution. F. Ö. acknowledges support of NSF Grant AST-9820686.

REFERENCES

Belloni, T., Zampieri, L., & Campana, S. 1997, A&A, 321, 835
Chakrabarty, D., Pivovaroff, M. J., Hernquist, L. E., Heyl, J. S., & Narayan, R. 2000, ApJ, submitted (astro-ph/0001026)
Chatarjee, P., Narayan, R., & Hernquist, L. E. 2000, ApJ, in press (astro-ph/9912137)
DeDeo, S., Psaltis, D., & Narayan, R. 2000, submitted (astro-ph/0004266)
Heyl, J., & Hernquist, L. E. 1998, MNRAS, 300, 599
Hurley, K. 2000, Astr. Let. Comm., in press (astro-ph/9912061)
Kaspi, V. M. 2000, in Pulsar Astronomy–2000 and Beyond, ASP Conf. Ser., in press (astro-ph/9912284)
Lattimer, J., & Prakash, 2000, ApJ, submitted (astro-ph/0002232)
Lewin, W. H. G., van Paradijs, J., & Taam, R. E. 1996, in X-ray Binaries, ed. W. H. G. Lewin, J. van Paradijs, & E. P. J. van den Heuvel (Cambridge, University Press)
Lyne, A., & Graham-Smith, F. 1990, Pulsars (Cambridge, University Press)
Mereghetti, S. Stella, L. 1995, ApJ, 442, L17
Miller, M. C., & Lamb, F. K. 1998, ApJ, 499, L37
Page, D. 1995, ApJ, 442, 273
Pavlov, G. G., Zavlin, V. E., Aschenbach, B., Trümper, J., & Sanwal, D. 2000, ApJ, 531, L53
Pavlov, G. G., Zavlin, V. E., Truemper, J. Neuhaeuser, R. 1996, ApJ, 472, L33
Pechenick, K. R., Ftaclas, C. Cohen, J. M. 1983, ApJ, 274, 846
Shaviv, N. J., Heyl, J. S., & Lithwick, Y. 1999, MNRAS, 306, 333
Strohmayer, T. E., Zhang, W., Swank, J. H., Smale, A., Titarchuk, L., Day, C., & Lee, U. 1996, ApJ, 469, L9
Strohmayer, T. E., Zhang, W., Swank, J. H., White, N. E., & Lapidus, I. 1998, ApJ, 498, L135
Sugizaki, M., et al. 1997, PASJ, 49, L25
Tananbaum, H. 1999, IAU Circ., No. 7246
Thompson, C., & Duncan, R. C. 1995, MNRAS, 275, 255
———. 1996, ApJ, 473, 322
van Paradijs, J., van den Heuvel, E. P. J., & Taam, R. 1996, A&A, 299, L41
Weinber, N., Miller, M. C., & Lamb, D. Q. 2000, ApJ, submitted (astro-ph/0001544)
Zavlin, V. E., Pavlov, G. G., & Trumper, J. 1998, A&A, 331, 821
Zavlin, V. E., Shibanov, Y. A., & Pavlov, G. G. 1995, Astr. Let., 21, 149
Zavlin, V. E., Trümper, J., Pavlov, G. G. 1999, ApJ, 525, 959